Robustness of the MAPK network topologies

Franco Blanchini* and Elisa Franco†

* Dipartimento di Matematica ed Informatica, Università degli Studi di Udine, Via delle Scienze 206, 33100 Udine, Italy: blanchini@uniud.it.

† Division of Engineering and Applied Science, California Institute of Technology, 1200 E. California Bl. Pasadena, CA 91125, USA: elisaf@caltech.edu

Abstract

In this paper we propose and analyze qualitative models of the mitogen-activated protein kinase (MAPK) pathway in a neural cell model organism. Experiments show that this MAPK pathway exhibits an input-dependent topology, leading to different dynamic behaviors of the pathway output and ultimately to different cell fates. Our analysis is based on invariant set theory and non-smooth Lyapunov functions. We demonstrate that the network behaviors and stability properties are structurally dependent on its topology, and do not depend on specific parameter values of the underlying biochemical interactions.

I. Introduction

One of the goals of systems biology is that of understanding how living organisms embed their functionalities in complex biochemical networks [1]. In terms of adaptability and robustness, such networks often outperform engineered devices, even though they exhibit remarkable intrinsic variability in their parameters and reagents concentrations. Well-known examples of robust biological networks include bacterial chemotaxis [2], [3] and [4]; the heat shock response in *E. coli* [5]; and bacterial phosphorylation cascades [6], [7].

A special class of phosphorylation cascades is given by the mitogen-activated protein kinase (MAPK) pathway. MAP kinases are proteins that respond to the binding of growth factors to cell surface receptors. The pathway consists of three enzymes, MAP kinase (MAP1K), MAP kinase kinase (MAP2K) and MAP kinase kinase kinase (MAP3K) that are activated in series following an upstream signaling event. This pathway is conserved across a large number of living organisms. Several studies have highlighted the presence of a positive feedback loop in the MAPK cascade and the consequent bi–stability of this system, which can generate switch-like and oscillatory responses [8]. A standard ODE model for a MAPK cascade found in *Xenopus* oocites is proposed in [9], where the authors demonstrated bi–stability of the system by applying the general theory of monotone systems [10]. In rat neural cells, the operation of the MAPK network has instead been shown to exhibit a context-dependent topology: two negative feedback loops are present in the network upon stimulation by epidermal growth factor (EGF), which then causes the cells to proliferate. Two positive feedback loops, and an additional negative loop, are instead present upon stimulation by neural growth factor (NGF), which then induces cell differentiation.

In this work, we consider the two input-dependent topologies experimentally investigated in [11]. Starting from our previous efforts in a parameter-free analysis of the MAPK pathway [12], we derive qualitative graphs describing the interactions of the MAPK reagents and propose a model for each of the two topologies. Under biologically plausible assumptions on the network interconnections, we analytically demonstrate that the qualitative dynamic behaviors of both topologies are structurally guaranteed. Specifically, such behaviors are independent of specific chemical interaction parameters. Thus, our results demonstrate that the MAPK cascade yields biologically robust behaviors, consistently with other results in the literature [13].

The mathematical tools employed to analyze and explain the robustness of biochemical systems encompass integral feedback [4], [5], linear matrix inequalities [14], structural analysis [15], Lyapunov methods [16] and the deficiency theory for chemical reaction networks [7], [17]. However, numerical analysis is often the preferred tool to explore parameter-independent, robust behaviors of biochemical systems [18], [19]. Throughout this work, we employ classical control theoretic tools such as set invariance and non-smooth Lyapunov functions, without resorting to any numerical simulation.

II. Modeling the MAPK pathway

In this section we provide further details on the biological significance of the MAPK pathway in PC12 cells, a useful model system to study neuronal differentiation. We then propose a general MAPK pathway dynamic model, which is consistent with the literature and can be constructed from qualitative graphs. The topology of the general model is finally modified to account for the additional input-dependent feedback loops determining the pathway response and ultimately the cell fate.

A. The MAPK pathway of PC12 cells exhibit a context-dependent topology

The MAPK pathway is a signaling cascade that has been conserved throughout evolution across a broad range of organisms from yeast to mammals. MAP kinases are proteins that respond to the binding of a variety of growth factors to cell surface receptors. The pathway consists of three enzymes, MAP3K, MAP2K and MAP1K that are activated in series. By activation or phosphorylation, we mean the addition of a phosphate group to the target protein. Extracellular signals can activate MAP3K, which in turn phosphorylates MAP2K at two different sites, forming species MAP2K-P and MAP2K-PP; in the last round, MAP2K phosphorylates MAP1K at two different sites, forming the species MAP1K-P and MAP1K-PP. The graphs of the network proposed in [11] and the well-known models in the literature [9], [8] prompted us to schematically represent the core behavior of the cascade as in Figure 1 A. Following a standard convention in the biology literature, the pointed arrows indicate that the end-species concentration increases upon increase of the source species; blunted arrows instead indicate a reduction of the end species caused by an increase in the source species. Solid lines indicate strong and statistically relevant interactions, while dashed lines indicate weak interactions. The solid “forward arrows” in the cascade denote the fact that upon external stimulation, the cascade equilibrium is naturally shifted to increase the concentration of MAP1K protein output. In the absence of additional feedback, this system has indeed been demonstrated to behave monotonically [10].

Rat adrenal pheochromocytoma (PC12) cells have been used as a model system to understand the relationship between their cellular fate and the MAPK signaling pathway operation [11]. The proteins involved in the PC12 MAPK pathway are Erk (MAP1K), Mek (MAP2K) and Raf (MAP3K). The MAP3K protein is activated by membrane sensing of external growth factors such as the Epidermal Growth Factor (EGF) or the Neuronal Growth Factor (NGF). Sensing of either of these growth factors triggers the previously mentioned MAPK activation cascade: however, EGF stimulation induces cellular proliferation, while NGF stimulation induces cell differentiation. The cell fate decision is correlated with a specific time response of the MAP1K protein Erk, the last element of the cascade [11]. Specifically, the time response of the MAP1K active protein concentration to EGF stimulation is a spike, followed by a relaxation to the initial, pre-stimulation amount of phosphorylated MAP1K: thus, the circuit is asymptotically stable at low MAP1K concentrations. The time response of active MAP1K to NGF stimulation is instead a sustained increase in concentration, even after NGF is removed: the network therefore exhibits bi-stability with hysteresis.

The authors of [11] investigated the MAPK pathway response focusing on its topology. Applying the Modular Response Analysis (MRA) technique [20] the network was systematically perturbed, allowing the derivation of local response coefficients describing the interactions between the kinases. The global steady state perturbations were measured with respect to the total concentrations of mono and bi-phosphorylated MAP kinases. The qualitative graphs derived in [11] are reproduced in Figure 1 C and G: solid lines correspond to local response coefficients measured with high probability across the experiments performed, while dashed lines correspond to coefficients inferred with low probability. In this work, we are not interested in the specific values of the local response coefficients, but rather on the qualitative dynamic interconnections that may underlie the measured responses. Figure 1 C shows that the EGF-stimulated network topology presents two strong negative feedback loops (solid red interconnections) in addition to the core MAPK pathway network (gray arrows, shown as in Figure 1 A); Figure 1 G shows that the NGF-stimulated network presents instead two strong positive feedback loops (solid green lines) and one strong negative feedback loop in addition to the core MAPK graph.

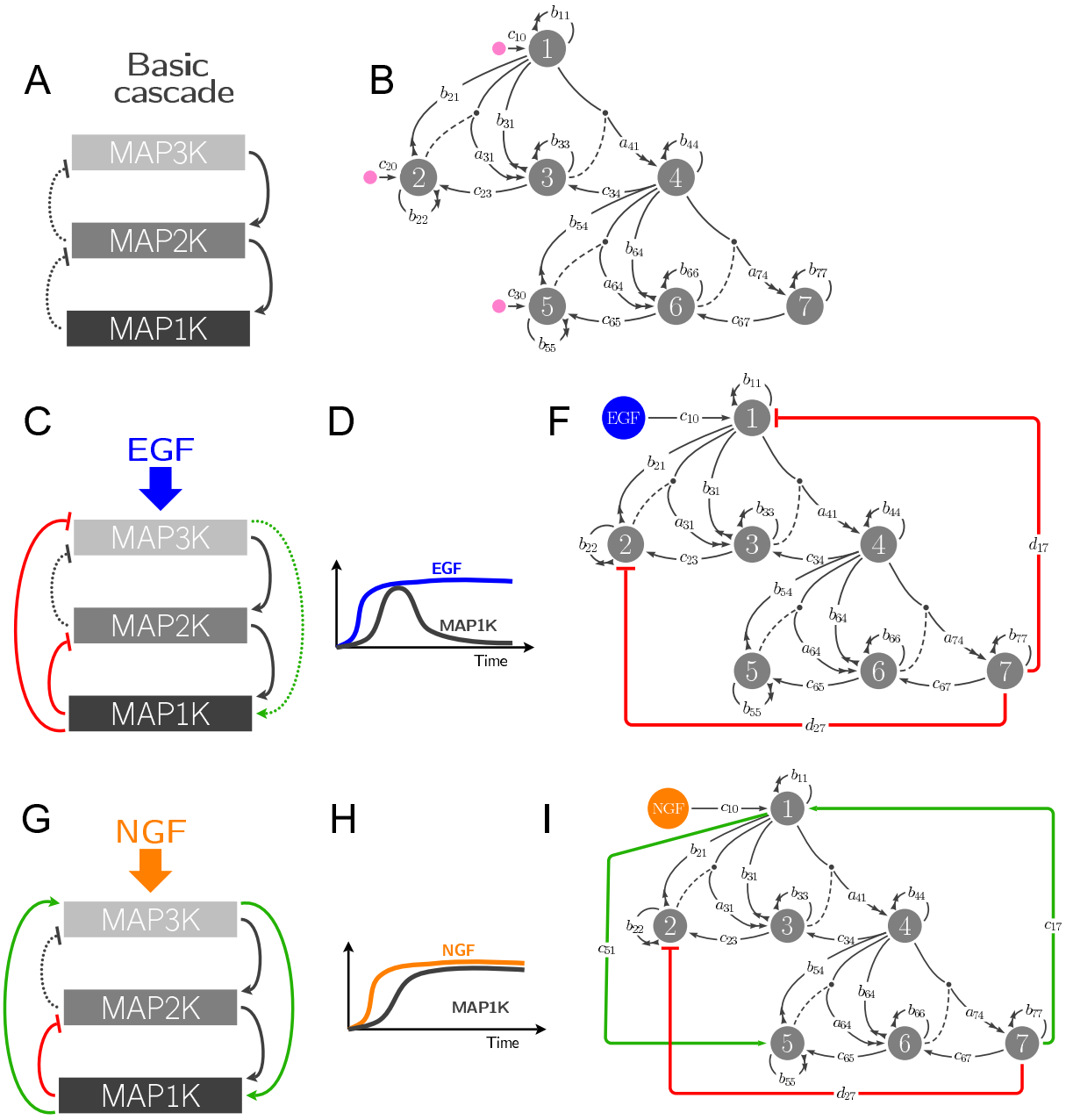

Fig. 1. **Topologies of the MAPK pathway considered in this paper A** Core pathway. **B** Topology induced by EGF input. **C** Topology induced by the NGF input.

B. Derivation of qualitative graphs and dynamic models for the MAPK topologies

In the remainder of this section, we propose a methodology to derive a dynamic model for each of these networks, based on biologically plausible interactions underlying the graph topologies. Let us refer to Table I and denote each species in the MAPK network as x_i, $i = 1, ..., 7$. We define a graph where the ith node is associated to species x_i, and every arc connecting nodes i and j is defined according to the qualitative dynamic interactions of the biological species x_i, x_j.

Given two nodes i and j, we say that "j affects i" if the derivative $\dot{x}_i(t)$ includes a function of x_j. Following the notation we introduced in a recent work [12], we classify the possible interactions in four categories.

TABLE I
DEFINITION OF THE STATE VARIABLES FOR THE MAPK NETWORK

x_1	x_2	x_3	x_4	x_5	x_6	x_7
MAP3K/Raf	MAP2K/Mek	MAP2K-P/Mek-P	MAP2K-PP/Mek-PP	MAPK/Erk	MAP1K-P/Erk-P	MAP1K-PP/Erk-PP

This categorization allows us to focus our analysis on fundamental functional relationships between the system variables, neglecting specific numerical parameters.

- a–interactions. This category includes positive activation dynamics, possibly unbounded, from species j to species i and is associated to functions of the form $a_{ij}(\cdot)x_i$. Note that $a_{ij}(\cdot)$ may be a function of one or more other species in the network. The arc type associated with this interaction is: $j \longrightarrow\!\!\!\!\rightarrow i$
- b–interactions. This category includes negative inhibition dynamics, possibly unbounded, from species j to species i and is associated to functions of the form $b_{ij}(\cdot)x_i$. The term $b_{ij}(\cdot)$ may be a function of one or more other species in the network; we assume $b_{ij}(0,\cdot) = 0$. Arc type: $j \longrightarrow\!\!\!\!\!\!\rightarrow i$
- c–interactions. This category includes increasing–but–bounded, positive activation dynamics caused by species j on species i and is associated to functions of the form $c_{ij}(x_j)$. Arc type: $j \longrightarrow i$
- d–interactions. This category includes decreasing, bounded, positive activation dynamics caused by species j on species i. This interaction type is associated to functions of the form $d_{ij}(x_j)$. Arc type: $j \longrightarrow\!\!\!\!\dashv i$

The "proportionality" coefficients a_{ij} and b_{ij} in the terms $a_{ij}(\cdot)x_j$ and $b_{ij}(\cdot)x_j$ are introduced to evidence the fact that the described phenomena may be far from linear, and the linear case is a possible specification of these terms.

The following definition will be useful in the sequel.

Definition 1: Function $f(x)$ is a sigmoidal function if it is non decreasing, if $f(0) = 0$, $f'(0) = 0$, $0 < f(\infty) < \infty$ and its derivative has a unique maximum point. Function $f(x)$ is a complementary sigmoidal function if $f(0) - f(x)$ is a sigmoid function.

Examples of sigmoidal and complementary sigmoidal functions are in Figure 2.

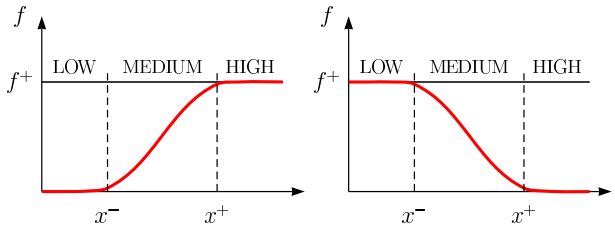

Fig. 2. Sigmoidal (left) and complementary sigmoidal (right) functions

Let us now derive a qualitative dynamical model of the MAPK pathway by restricting our attention to the simple cascade of Figure 1 A. We will derive a slightly more complex graph, shown in Figure 1 B, by incorporating more biological information in the system description. We assume that MAP(i)K, where $i = 1, 2, 3$, is produced and degraded at some rate. Referring to the graph in Figure 1 B, and based on the four interaction categories previously introduced, we can associate the production of each species to a positive and bounded activation function of type c_{i0}; degradation can be plausibly associated to a function $b_{ii}(x_i)x_i$. Each MAP(i)K, for $i = 2, 3$, mediates the phosphorylation of MAP($i-1$)K through a Hill-type activation process, transforming it into a MAP($i-1$)K-P, phosphorylated at a single site; additionally, MAP(i)K mediates the addition of a second phosphate group, transforming MAP($i-1$)K-P into MAP($i-1$)K-PP. Consider the nodes of the graph at Figure 1 B associated to x_1, x_2 and x_3: it is natural to connect nodes x_1 and x_3 with a function of type $a_{13}(x_2)x_3$. Similarly for x_1 and x_4, and for activation of x_6, x_7 by x_4. Due to mass conservation, if MAP(i)K causes the increase of MAP($i-1$)K-P and MAP($i-1$)K-PP, then MAP(i)K also causes a decrease of MAP($i-1$)K and MAP($i-1$)K-P: this effect is taken into account by the arcs b_{21}, b_{31}, b_{54} and b_{64} in Figure 1 B. Furthermore, one can assume a spontaneous loss of phosphate groups: MAP(i)K-P and MAP(i)K-PP decay into MAP(i)K

and MAP(i)K-P respectively (mass conservation still holds). This bounded decay effect is taken into account, together with other kinase degradation processes, by arcs b_{33}, b_{44}, b_{66} and b_{77}; the simple loss of a phosphate group causes a bounded increase of the concentration of MAP(i)K and MAP(i)K-P, taken into account through the arcs c_{23}, c_{34}, c_{56} and c_{67}. We ignore the input-mediated phosphorylation dynamics of the MAP3K protein, as done for instance in [9].

The graphs in Figure 1 A and B are derived with different procedures. However, both graphs aim at representing the same underlying positively and negatively correlated dynamic interactions among the kinases, with different levels of complexity. From the detailed graph in Figure 1 B, a dynamic model can be immediately written as follows:

$$\begin{aligned}
\dot{x}_1 &= +c_{10} - b_{11}(x_1)x_1 \\
\dot{x}_2 &= -b_{21}(x_2)x_1 - b_{22}(x_2)x_2 + c_{23}(x_3) + c_{20} \\
\dot{x}_3 &= a_{31}(x_2)x_1 - b_{31}(x_3)x_1 - b_{33}(x_3)x_3 + c_{34}(x_4) \\
\dot{x}_4 &= a_{41}(x_3)x_1 - b_{44}(x_4)x_4 \\
\dot{x}_5 &= +c_{50} - b_{54}(x_5)x_4 - b_{55}(x_5)x_5 + c_{56}(x_6) \\
\dot{x}_6 &= a_{64}(x_5)x_4 - b_{64}(x_6)x_4 - b_{66}(x_6)x_6 + c_{67}(x_7) \\
\dot{x}_7 &= a_{74}(x_6)x_4 - b_{77}(x_7)x_7.
\end{aligned} \tag{1}$$

The following qualitative properties are assumed. All functions are nonnegative. Functions $b_{11}(x_1)x_1$, $b_{22}(x_2)x_2$, $b_{33}(x_3)x_3$ and $b_{44}(x_4)x_4$, $b_{54}(x_5)$, $a_{74}(x_6)$ and $b_{77}(x_7)x_7$ functions $c_{23}(x_3)$, $b_{21}(x_2)$, $a_{41}(x_3)$, and functions $c_{56}(x_6)$, $b_{54}(x_5)$, $a_{74}(x_6)$ are assumed strictly increasing with positive derivative. Furthermore, all these function are null at zero. Mass conservation allows us to assume the following equalities: $a_{31}(x_2) = b_{21}(x_2)$, $c_{34}(x_4) = b_{44}(x_4)x_4$, $b_{31}(x_3) = a_{41}(x_3)$, $b_{33}(x_3)x_3 = c_{23}(x_3)$ and $a_{64}(x_5) = b_{54}(x_5)$, $c_{67}(x_7) = b_{77}(x_7)x_7$, $b_{64}(x_6) = a_{74}(x_6)$, $b_{66}(x_6)x_6 = c_{56}(x_6)$. The degradation of x_4 and x_3 is given by the loss of a phosphate group and decay to x_3 and x_2. (Similarly for x_7 and x_6, turning into x_6 and x_5 respectively.) Conversely x_2 and x_5 have their own degradation given by terms $b_{22}(x_2)x_2$ and $b_{55}(x_5)x_5$. The terms c_{10}, c_{20} and c_{50} are non–negative constants.

The literature provides several well-known ordinary differential equations models describing the phosphorylation process at each node of the cascade. In particular, the derivation of our model was aided by the biological assumptions made in [9]. Our model is indeed consistent with the one proposed in [9], as we outlined also in our previous work [12].

In the next sections we will consider the two different topologies for the PC12 MAPK pathway that have been shown to arise upon stimulation by EGF and NGF input signals.

III. EGF INDUCED MAPK TOPOLOGY

According to [11], when stimulated with EGF the MAPK topology presents two strong negative feedback loops between the MAPK and the MAP2K proteins, and between the MAPK and MAP3K proteins. The corresponding dynamic behavior of the MAPK output (x_7) is a characteristic spike, as schematically shown in Figure 1 D. We chose to neglect the positive feedback loop between the MAP3 and the MAP kinases, because it is statistically insignificant according to [11]. We propose to model the negative feedback loops as positive, decreasing and bounded interactions of type $d_{ij}(\cdot)$, mediated by the doubly phosphorylated form of the MAPK protein, x_7. The graph is shown in Figure 1 F. The qualitative ODE model can be straightforwardly derived from the graph

as follows:

$$\begin{aligned}
\dot{x}_1 &= +c_{10} - b_{11}(x_1)x_1 + d_{17}(x_7) \\
\dot{x}_2 &= -b_{21}(x_2)x_1 - b_{22}(x_2)x_2 + c_{23}(x_3) + d_{27}(x_7) \\
\dot{x}_3 &= a_{31}(x_2)x_1 - b_{31}(x_3)x_1 - b_{33}(x_3)x_3 + c_{34}(x_4) \\
\dot{x}_4 &= a_{41}(x_3)x_1 - b_{44}(x_4)x_4 \\
\dot{x}_5 &= +c_{50} - b_{54}(x_5)x_4 - b_{55}(x_5)x_5 + c_{56}(x_6) \\
\dot{x}_6 &= a_{64}(x_5)x_4 - b_{64}(x_6)x_4 - b_{66}(x_6)x_6 + c_{67}(x_7) \\
\dot{x}_7 &= a_{74}(x_6)x_4 - b_{77}(x_7)x_7
\end{aligned} \tag{2}$$

The functional properties of the ODE terms are defined as for the general model (1). In addition, we assume that terms $d_{27}(x_7)$ (which substitutes and comprises the term c_{20} in model (1), accounting for the influence of x_7) $d_{14}(x_4)$ are strictly decreasing, with negative derivative; these terms may naturally be represented by complementary sigmoidal functions, however this is not a necessary assumption.

Term d_{27} is a complementary sigmoidal function (see Figure (2) right) which is assumed to be constant below some threshold, and null above some second threshold.

$$\begin{aligned}
&d_{27}(x_7) = d_{27}(0) \doteq \theta, \qquad \text{for} \qquad x_7 \leq \eta \\
&d_{27}(x_7) = 0, \qquad\qquad\quad \text{for} \qquad x_7 \geq \xi,
\end{aligned}$$

This special assumption is introduced to explain the "spiking" nature of the system in a reasonably simple way.

Term $b_{11}(x_1)x_1$ has a positive derivative and is unbounded (such as $b_{11}x_1$ with constant $b_{11} > 0$). This assumption is necessary to consider arbitrarily large external signals.

A. Steady state analysis of the EGF-induced MAPK topology

In this section, we will first derive qualitative steady state expressions for x_4 and x_7 (the doubly-phosphorylated kinases) as a function of the input. We will then prove the uniqueness of the equilibrium. We will provide, in passing, useful information for the next subsection.

The steady state conditions are achieved by assuming $\dot{x}_1 = 0$. Let us consider the first four equations and write them as follows

$$+ c_{10} - b_{11}(x_1)x_1 = -d_{17}(x_7) \tag{3}$$

$$-b_{21}(x_2)x_1 - b_{22}(x_2)x_2 + c_{23}(x_3) = -d_{27}(x_7) \tag{4}$$

$$a_{31}(x_2)x_1 - b_{31}(x_3)x_1 - b_{33}(x_3)x_3 + c_{34}(x_4) = 0 \tag{5}$$

$$a_{41}(x_3)x_1 - b_{44}(x_4)x_4 = 0 \tag{6}$$

In view of the equality assumptions, the condition

$$\dot{x}_2 + \dot{x}_3 + \dot{x}_4 = 0$$

becomes

$$- b_{22}(x_2)x_2 + d_{27}(x_7) = 0 \tag{7}$$

For a fixed input c_{10} equations (3)–(6) give, in an implicit form, x_1, x_2, x_3 and x_4 as functions of x_7 and c_{10}.

Lemma 1: We can express the steady state of x_4 as:

$$x_4 = \varphi(x_7, c_{10}) \tag{8}$$

Function φ is well–defined. It is decreasing with respect to x_7 and increasing with respect c_{10}.

The proof is reported in the appendix.

Let us now consider the equations $\dot{x}_5 = 0$, $\dot{x}_6 = 0$ and $\dot{x}_7 = 0$ written as follows

$$\begin{aligned} 0 &= +c_{50} - b_{54}(x_5)x_4 - b_{55}(x_5)x_5 + c_{56}(x_6) && (9)\\ 0 &= a_{64}(x_5)x_4 - b_{64}(x_6)x_4 - b_{66}(x_6)x_6 + c_{67}(x_7) && (10)\\ 0 &= a_{74}(x_6)x_4 - b_{77}(x_7)x_7 && (11) \end{aligned}$$

Summing them up as $\dot{x}_5 + \dot{x}_6 + x_7 = 0$, and eliminating the equal terms, we get

$$-b_{55}(x_5)x_5 + c_{50} = 0 \tag{12}$$

We can now state a second lemma.

Lemma 2: We can express the steady state of x_7 as:

$$x_7 = \psi(x_4, c_{50}). \tag{13}$$

Function ψ is well–defined and increasing in both variables.

Proof It is immediately seen that given c_{50}, x_5 is given by (12), and given x_4, x_6 is uniquely defined by (9). x_7 is determined by (11). For fixed c_{50}, x_5 is fixed. If x_4 grows, (9) implies that x_6 grows. Then x_7 grows in view of (11). Similarly, if x_4 is fixed, increasing c_{50} increases x_5 by (12). From (9) and (12), we have that x_6 increases. From (11) we see that x_7 also grows. □

Remark 1: It is legitimate to assume [9] that the amount $x_5 + x_6 + x_7 = \zeta$ is constant (or varying on a much slower timescale than the cascade dynamics). We can therefore consider a reduced system with variables x_5, x_7, with $x_6 = \zeta - x_5 - x_7$. At steady-state, $\dot{x}_5 = 0$, $\dot{x}_7 = 0$, namely

$$\begin{aligned} 0 &= +c_{50} - b_{54}(x_5)x_4 - b_{55}(x_5)x_5 + c_{56}(\zeta - x_5 - x_7)\\ 0 &= a_{74}(\zeta - x_5 - x_7)x_4 - b_{77}(x_7)x_7 \end{aligned}$$

Then it can be shown that in this case x_7 is an increasing function of x_4. This same property will be proved for the NGF-induced topology, in Lemma 4.

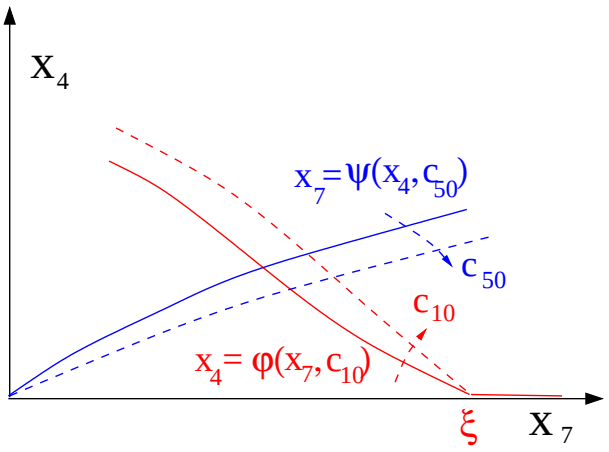

Fig. 3. The intersection between $x_4 = \varphi(x_7)$ and $x_7 = \varphi(x_4)$

Combining Lemmas 1 and 2 we have the following.

Proposition 1: For fixed values of the input c_{10} and c_{50} there can be at most one equilibrium point. The equilibrium value of $\bar{x}_7$ is an increasing function of both c_{10} and c_{50}.

Proof The equilibrium condition are achieved by the two conditions

$$x_4 = \varphi(x_7, c_{10}) \tag{14}$$

$$x_7 = \psi(x_4, c_{50}). \tag{15}$$

The qualitative behavior of the functions above is sketched in Figure 3. Since φ is decreasing and ψ is increasing, the first part of the proof is immediate.

For the second part of the proof note that in view of (14) if c_{10} increases for fixed c_{50}, either x_4 or x_7 must increase. If x_7 increases, the proof is complete. If x_4 increases, then also x_7 increases because of (15) and Lemma 2. Conversely if c_{50} increases, given c_{10}, then equation (15) implies that either x_7 increase, as we wish to prove, or x_4 decreases. In the latter case x_7 increases, as a consequence of (14) Lemma 1. □

In essence, increasing c_{50} shifts the ψ–curve downward, and increasing c_{10} shifts the φ–curve upwards.

The following proposition completes the steady–state analysis

Proposition 2: There are no equilibria in the high region $x_7 \geq \xi$.

The proposition is due to the fact that $\varphi(x_7, c_{10}) = 0$ for $x_7 \geq \xi$ and an immediate consequence of the next Lemma 3.

B. The dynamic response of the MAP1K concentration to a step in EGF concentration is robustly characterized by a spike followed by a relaxation to the initial, pre-stimulus equilibrium.

The following lemma is a key step to prove that for c_{10} large enough, $x_7(t)$ exhibits an overshoot (spike) followed by a relaxation to the unique equilibrium. In simple words, this lemma states that if the MAP1K-PP concentration x_7 achieves values above the threshold ξ, then its concentration will necessarily decrease below ξ after some time.

Lemma 3: Assume that at a certain time $\bar{t} > 0$, $x_7(\bar{t}) > \xi$. Then there necessarily exists $t > \bar{t}$ such that $x_7(t) \leq \xi$.

Proof Assume by contradiction that $x_7(t) > \xi$ for all $t > \bar{t}$. Define the variable

$$\kappa(t) \doteq x_2(t) + x_3(t) + x_4(t) \tag{16}$$

which, in view of the equality assumptions, satisfies the equation

$$\dot{\kappa} = -b_{22}(x_2)x_2 + d_{27}(x_7) \tag{17}$$

Since we assume that $d_{27}(x_7) = 0$ for $x_7 \geq \xi$, we have $\dot{\kappa} = -b_{22}(x_2)x_2$, which implies that κ is monotonically non–increasing and it converge to $\bar{\kappa} > 0$ from above and and also $\dot{\kappa} \to 0$. From (17) this means $x_2(t) \to 0$.

Consider the equation of $\dot{x}_2$

$$\dot{x}_2 = -b_{21}(x_2)x_1 - b_{22}(x_2)x_2 + c_{23}(x_3)$$

Since x_2 and $\dot{x}_2$ converge to zero, $c_{23}(x_3)$ converges also to zero, hence $x_3(t)$ converges to zero. Consider the equation for $\dot{x}_4$.

$$\dot{x}_4 = a_{41}(x_3)x_1 - b_{44}(x_4)x_4$$

Since $x_3(t) \to 0$ asymptotically we have $\dot{x}_4 = -b_{44}(x_4)x_4$, which implies that $x_4(t) \to 0$. Then $\kappa = x_2(\infty) + x_3(\infty) + x_4(\infty) = 0$.

Consider the equation for $\dot{x}_7$

$$\dot{x}_7 = a_{74}(x_6)x_4 - b_{77}(x_7)x_7$$

The conditions $x_4(t) \to 0$ leads to $\dot{x}_7 = -b_{77}(x_7)x_7 \leq -b_{77}(\xi)\xi$ as long as $x_7(t) \geq \xi$. Then for t large enough, will reach a value $x_7(t) \leq \xi$ □

It is harder to demonstrate that if c_{10} large enough, x_7 has robustly exhibits an overshoot. This can be shown only if $d_{27}(0) = \theta$ is sufficiently large. We introduce the following additional assumptions:

A1) The production and degradation for x_5 cancel each other, and we can assume mass conservation of the MAP1K protein [9]. This allows us to remove the terms $b_{55}(x_5)x_5$ and c_{50}. The dynamics of x_5 are therefore:

$$\dot{x}_5 = -b_{54}(x_5)x_4 + c_{56}(x_6). \tag{18}$$

Accordingly we can eliminate the argument c_{50} from ψ in the steady state expression (13):

$$x_7 = \psi(x_4). \tag{19}$$

Assumption A1 allows us to complete easily our analysis; we conjecture that this assumption may be removed. This assumption is equivalent to assuming mass conservation:

$$\dot{x}_5 + \dot{x}_6 + \dot{x}_7 = 0,$$
$$x_5(t) + x_6(t) + x_7(t) = \zeta = const. \tag{20}$$

A2) Define $\kappa(0) \doteq x_2(0) + x_3(0) + x_4(0)$, such that for a given ζ,

$$\psi(\kappa(0)) > \xi$$

where ψ is the equilibrium condition in (19).

Assumption A2 basically means that the two chains are initially charged enough in terms of $\kappa = x_2 + x_3 + x_4$ and $\zeta = x_5 + x_6 + x_7$ in order to be able to "boost" a spike for x_7.

A3) $x_7(0) < \eta$.

The last assumption just means that the system is initialized in the "low level region".

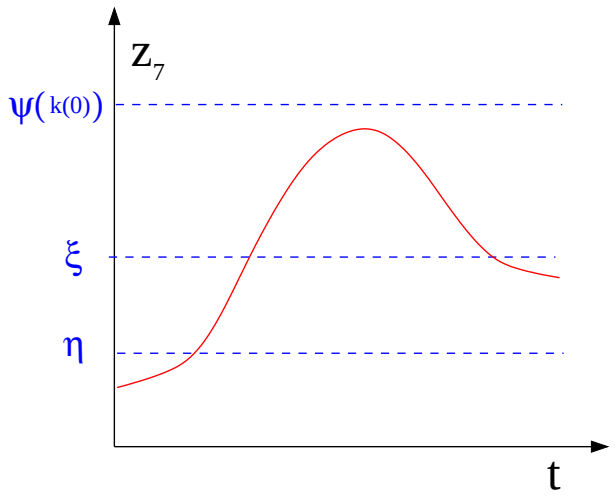

Fig. 4. Qualitative overshoot and relaxation behavior exhibited by the EGF-induced MAPK pathway.

Theorem 1: i) Under Assumptions A1), A2) A3) and for c_{10} large enough there is a peak in the sense that $x_7(t)$ rises over ξ and then comes back below (see Fig 4).
ii) Such a peak is upper bounded by (but arbitrarily close to) $\psi(\kappa(0))$.

Proof In view of Lemma (3) we need just to prove that $x(7)$ at some time reaches a value arbitrarily close, but below $\psi(\kappa(0))$.

As a first step, we observe that x_1 can grow arbitrarily large in an arbitrarily small time for C_{10} large enough. From:

$$\dot{x}_1 = +c_{10} - b_{11}(x_1)x_1 + d_{17}(x_7) \geq +c_{10} - b_{11}(x_1)x_1,$$

we have that for arbitrary small $\tau_1 > 0$ and for any arbitrary $\mu > 0$, $x_1(t) > \mu$ for $t \geq \tau_1$.

For $t \geq \tau_1$, in view of the equation for $\dot{x}_2$

$$\dot{x}_2 = -b_{21}(x_2)x_1 - b_{22}(x_2)x_2 + c_{23}(x_3) + d_{27}(x_7) \leq -b_{21}(x_2)x_1 + c_{23}(0) + d_{27}(0)$$

and, since $x_1 \geq \mu$ can be arbitrarily large after arbitrarily small $\tau_2 > \tau_1$ $x_2(t)$ can be made arbitrarily small,

$$x_2(t) \leq \epsilon_2. \quad \text{for} \quad t \geq \tau_2$$

Now consider the variable $\kappa(t) = x_2(t) + x_3(t) + x_4(t)$, defined in (16) satisfying equation (17). κ is non–increasing and it decreasing can be made arbitrarily slow. For $t \geq \tau_2$

$$\dot{\kappa} = \dot{x}_2 + \dot{x}_3 + \dot{x}_4 = -b_{22}(x_2)x_2 \geq -b_{22}(\epsilon_2)\epsilon_2$$

Then, for $t \geq \tau_2$

$$\kappa(t) \geq \kappa(\tau_2) - [b_{22}(\epsilon_2)\epsilon_2](t - \tau_2)$$

From (17) $\dot{\kappa} \leq d_{27}(0)$, then κ is upper bounded: $\kappa(t) \leq \kappa(0) + t d_{27}(0)$. On $[0, \tau_2]$, $\kappa(t) \leq \kappa(0) + \epsilon_2 d_{27}(0) \doteq \bar{\kappa}_2$ Then $x_2(t) \leq \kappa(t) \leq \bar{\kappa}_2$ on $[0, \tau_2]$. On the other hand, $\dot{\kappa} \geq -b_{22}(x_2)x_2$ thus we have

$$\kappa(\tau_2) \geq \kappa(0) - b_{22}(\bar{\kappa}_2)\bar{\kappa}_2\tau_2.$$

Combining the two bounds we get, for $t \geq \tau_2$,

$$\kappa(t) \geq \kappa(0) - b_{22}(\bar{\kappa}_2)\kappa_2\tau_2 - [b_{22}(\epsilon_2)\epsilon_2](t - \tau_2)$$

Since τ_2 and ϵ_2 can be arbitrarily small this is equivalent to say that κ can be sustained arbitrarily close to $\kappa(0)$ for an arbitrary large period, precisely, given an arbitrary large T and ϵ_κ, there exists c_{10} such that

$$\kappa(t) \geq \kappa(0) - \epsilon_\kappa, \qquad \text{for all} \quad 0 \leq t \leq T$$

Let us now consider x_4 whose equation is $\dot{x}_4 = a_{41}(x_3)x_1 - b_{44}(x_4)x_4$. For $\tau_2 \leq t \leq T$. Remembering that $x_1 \geq \mu$

$$\dot{x}_4 \geq a_{41}(\kappa(t) - x_2 - x_4(t))x_1 - b_{44}(x_4)x_4 \geq a_{41}\,(\ \max\{0, \kappa(0) - \epsilon_\kappa - \epsilon_2 - x_4(t)\}\ )\,\mu - b_{44}(x_4)x_4$$

This inequality implies that for μ arbitrarily large, the argument $\max\{0, \kappa(0) - \epsilon_\kappa - \epsilon_2 - x_4(t)\}$ of a_{41}, must converge to zero arbitrarily fast. Thus given $\tau_4 > \tau_2$ with $\tau_4 - \tau_2$ arbitrarily small and given ϵ_4 arbitrarily small, the condition

$$x_4(t) \geq \kappa(0) - \epsilon_\kappa - \epsilon_2 - \epsilon_4 \doteq \bar{x}_4, \quad \text{for} \quad \tau_4 \leq t \leq T$$

Note that, by continuity, being the "epsilons" small, the following condition can be granted

$$\bar{x}_7 \doteq \psi(\bar{x}_4) > \xi$$

which is a key point of the proof.

We need now to show that $x_7(t)$ converges, either in finite time or asymptotically to $\bar{x}_7 > \xi$. To this aim we consider the second chain x_5–x_6–x_7, and we eliminate $x_6 = \zeta - x_5 - x_7$ (see eq. (20))

$$\dot{x}_5 = -b_{54}(x_5)x_4 + c_{56}(\zeta - x_5 - x_7) \tag{21}$$

$$\dot{x}_7 = a_{74}(\zeta - x_5 - x_7)x_4 - b_{77}(x_7)x_7 \tag{22}$$

The equilibrium conditions which link $\bar{x}_4$ to $\bar{x}_7 = \psi(\bar{x}_4)$ are

$$0 = -b_{54}(\bar{x}_5)\bar{x}_4 + c_{56}(\zeta - \bar{x}_5 - \bar{x}_7) \tag{23}$$

$$0 = a_{74}(\zeta - \bar{x}_5 - \bar{x}_7)\bar{x}_4 - b_{77}(\bar{x}_7)\bar{x}_7. \tag{24}$$

We use the Lyapunov–like piecewise affine function (see Figure 5)

$$V(x_5 - \bar{x}_5, x_7 - \bar{x}_7) = \max\{x_5 - \bar{x}_5, \bar{x}_7 - x_7, 0\} \tag{25}$$

which is zero only for $x_5 \leq \bar{x}_5$ and $x_7 \geq \bar{x}_7$. For $\tau_4 \leq t \leq T$ such a function is either decreasing or zero.

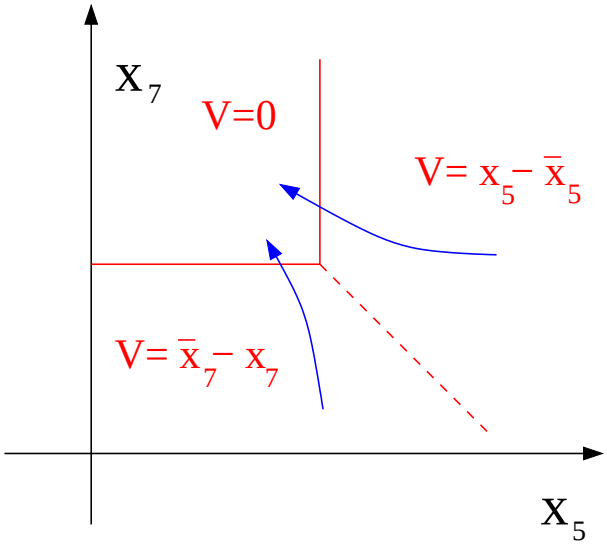

Fig. 5. Qualitative representation of the Lyapunov function (25)

For $x_5 - \bar{x}_5 > \bar{x}_7 - x_7$, namely, $x_5 + x_7 \geq \bar{x}_5 + \bar{x}_7$ (in the right sector in Figure 5) by taking into account (21) and (23) we have

$$\dot{x}_5 = -b_{54}(x_5)x_4 + c_{56}(\zeta - x_5 - x_7) = -b_{54}(x_5)x_4 + b_{54}(\bar{x}_5)\bar{x}_4 + c_{56}(\zeta - x_5 - x_7) - c_{56}(\zeta - \bar{x}_5 - \bar{x}_7) < 0$$

thus $V = x_5 - \bar{x}_5$ is decreasing

For $x_5 - \bar{x}_5 < \bar{x}_7 - x_7$, namely, $x_5 + x_7 \leq \bar{x}_5 + \bar{x}_7$ (in the lower sector in Figure 5) by taking into account (22) and (24) we have

$$\dot{x}_7 = a_{74}(\zeta - x_5 - x_7)x_4 - b_{77}(x_7)x_7 = a_{74}(\zeta - x_5 - x_7)x_4 - a_{74}(\zeta - \bar{x}_5 - \bar{x}_7)\bar{x}_4 - b_{77}(x_7)x_7 + b_{77}(\bar{x}_7)\bar{x}_7 > 0$$

Thus $V = \bar{x}_7 - x_7$ is decreasing.

Since the horizon T can be arbitrarily large, $(x_5(t), x_7(t))$ "has the time to approach" the region in which $V = 0$ (top–left sector in Figure 5), and then x_7 has the time to arbitrarily approach $\bar{x}_7$ thus exceeding ξ, and this concludes the proof. □

Remark 2: No stability of the unique equilibrium has been proven. However we claim that in the low region $x_7 < \eta$ the equilibrium is stable. This can be proven using the same machinery adopted in the next section.

IV. NGF MAPK TOPOLOGY

When stimulated with NGF the MAPK topology presents strong positive feedback loops between the MAPK and the MAP3K proteins, and a strong negative interaction between the MAPK and MAP2K proteins. We recall that the behavior of the MAPK output (x_7) is bistable, as schematically shown in Figure 1 H. Additionally, the experiments in [11] show that the system exhibits hysteresis upon removal of the NGF input. We propose to model the positive feedback loops as positive, increasing and bounded interactions of $c-$type mediated by the doubly phosphorylated forms of the kinases x_1 and x_7. The negative interaction between the MAPK and MAP2K proteins is hypothesized to be a $d-$type term that acts on the unphosphorylated MAP2K variable x_2.

The corresponding graph is shown in Figure 1 I. The resulting NGF-induced MAPK network is thus described by the following equations:

$$\begin{aligned}
\dot{x}_1 &= +c_{17}(x_7) + c_{10} - b_{11}(x_1)x_1 && (26)\\
\dot{x}_2 &= c_{23}(x_3) - b_{21}(x_2)x_1 - b_{22}(x_2)x_2 + d_{27}(x_7) && (27)\\
\dot{x}_3 &= a_{31}(x_2)x_1 + c_{34}(x_4) - b_{31}(x_3)x_1 - b_{33}(x_3)x_3 && (28)\\
\dot{x}_4 &= a_{41}(x_3)x_1 - b_{44}(x_4)x_4 && (29)\\
\dot{x}_5 &= c_{56}(x_6) - b_{54}(x_5)x_4 + c_{51}(x_1) - b_{55}(x_5)x_5 && (30)\\
\dot{x}_6 &= a_{64}(x_5)x_4 + c_{67}(x_7) - b_{64}(x_6)x_4 - b_{66}(x_6)x_6 && (31)\\
\dot{x}_7 &= a_{74}(x_6)x_4 - b_{77}(x_7)x_7. && (32)
\end{aligned}$$

We assume the same functional qualitative properties as in the general model (1). The terms $d_{27}(x_7)$ is again assumed to be strictly decreasing, with negative derivative. Term $b_{11}(x_1)x_1$ has a positive derivative and is unbounded (such as $b_{11}x_1$ with constant $b_{11} > 0$). This assumption is necessary to consider arbitrarily large external signals.

The following specific assumptions are further made. Term $c_{51}(x_1)$ is strictly increasing, with positive derivative and bounded (typically a sigmoidal–like functions).

Term c_{17} is a sigmoidal function (see Figure (2)) which is exactly null and exactly constant below and above some thresholds

$$\begin{aligned}
c_{17}(x_7) &= 0, \qquad \text{for} \quad x_7 \leq \eta\\
c_{17}(x_7) &= c_{17}(0), \qquad \text{for} \quad x_7 \geq \xi,
\end{aligned}$$

This special assumption is introduced to explain the "bi stability with hysteresis" nature of the system in a reasonably simple way.

Finally we introduce assume that the generation term for variable x_2 matches its degradation. This is equivalent to assuming mass conservation for the MAP2K protein concentration [9]. This allows us to remove the terms $b_{22}(x_2)x_2$ and $d_{27}(x_7)$ and to consider the simplified x_2 dynamics:

$$\dot{x}_2 = c_{23}(x_3) - b_{21}(x_2)x_1.$$

Moreover:

$$x_2(t) + x_3(t) + x_4(t) = \kappa = \text{constant}. \tag{33}$$

A. Steady state analysis of the NGF MAPK topology

As done for the EGF-induced pathway, we begin our analysis by looking for an expression of the steady state as a function of variables x_1 and x_7.

Given x_1 the two conditions $\dot{x}_2 = 0$ $\dot{x}_4 = 0$, equivalent to (in view of (33))

$$\begin{aligned}
-b_{21}(x_2)x_1 + c_{23}(k - x_2 - x_4) &= 0 && (34)\\
a_{41}(k - x_2 - x_4)x_1 - b_{44}(x_4)x_4 &= 0 && (35)
\end{aligned}$$

These equations implicitly define the equilibrium of x_4 as a function of x_1 and of the total available amount of MAP2K.

Lemma 4: The steady state of x_4 can be expressed as:

$$x_4 = \varphi_{4,1k}(x_1, \kappa). \tag{36}$$

Function $\varphi_{4,1k}(x_1, \kappa)$ is well defined and increasing in both arguments.

The proof is reported in the appendix. Let us now define the variable

$$x_5(t) + x_6(t) + x_7(t) = \zeta(t) \tag{37}$$

which satisfies, in view of the equality assumptions in Subsection II-B, the equation

$$\dot{\zeta} = c_{51}(x_1) - b_{55}(x_5)x_5. \tag{38}$$

Consider the steady–state equations $\dot{x}_5 = 0$, $\dot{x}_7 = 0$ and $\dot{\zeta} = 0$

$$\begin{aligned} c_{56}(x_6) - b_{54}(x_5)x_4 + c_{51}(x_1) - b_{55}(x_5)x_5 &= 0 & (39)\\ a_{74}(x_6)x_4 - b_{77}(x_7)x_7 &= 0 & (40)\\ c_{51}(x_1) - b_{55}(x_5)x_5 &= 0 & (41) \end{aligned}$$

These equations allow to state another lemma.

Lemma 5: The equilibria of x_7 can be expressed implicitly as:

$$x_7 = \varphi_{7,14}(x_1, x_4). \tag{42}$$

Function $\varphi_{7,14}(x_1, \kappa)$ is well defined and increasing in both arguments.

Proof Given x_1, (41) determines x_5 and, given x_4, (39) determines x_6. Finally, (40) determines x_7.

It is easy to see that if x_1 increases (and x_4 does not decrease) then x_5 increases from (41). In view of (41) rewrite (39) as

$$c_{56}(x_6) - b_{54}(x_5)x_4 = 0$$

then x_6 increases. From (40) x_7 increases. If x_4 increase and x_1 does not decrease, x_5 does not decrease, the last equation implies that x_6 increases. From (40) x_7 increases. □

Combining the lemmas we have the following propositions.

Proposition 3: The composed function defined as

$$\varphi(x_1, \kappa) \doteq \varphi_{7,14}\left(x_1, \varphi_{4,1k}(x_1, \kappa)\right) \tag{43}$$

is well defined an increasing in both argument. Moreover for fixed $\kappa > 0$

$$\lim_{x_1 \to \infty} \varphi(x_1, \kappa) \doteq \rho_\kappa < 0.$$

Proof The proof of the first part of the proposition is immediate. The second part can be easily proved noting that that $c_{51}(x_1)$ is bounded, and that x_4 is upper bounded by κ due to expression (33). Indeed, $\lim_{x_1 \to \infty} \varphi_{4,1k}(x_1, \kappa) = \kappa$. □

Consider now the steady state equation $\dot{x}_1 = 0$ written as:

$$c_{17}(x_7) + c_{10} = b_{11}(x_1)x_1$$

From this equation we implicitly derive a function

$$x_1 = \psi(x_7, c_{10}) \tag{44}$$

as the unique solution of the equation. Such a function is obviously non–decreasing. It is not difficult to see that, for fixed c_{10}, if is a sigmoid plus a constant and *satisfies essentially the same assumption* of $c_{17}(x_7)$, being constant below η and above ξ. Both functions φ and ψ are depicted in Figure 6. We are in the position of drawing the following conclusions.

- Curve $x_7 = \varphi(x_1, \kappa)$ has a vertical asymptote which is moved on the right if κ is augmented. The curve $x_7 = \psi(x_7, c_{10})$ is raised by augmenting c_{10}.
- For small κ there is a single equilibrium which is non–trivial if and only if $c_{10} > 0$. In particular for $\rho_\kappa \leq \eta$ there is a single intersection (point A in Figure 6).

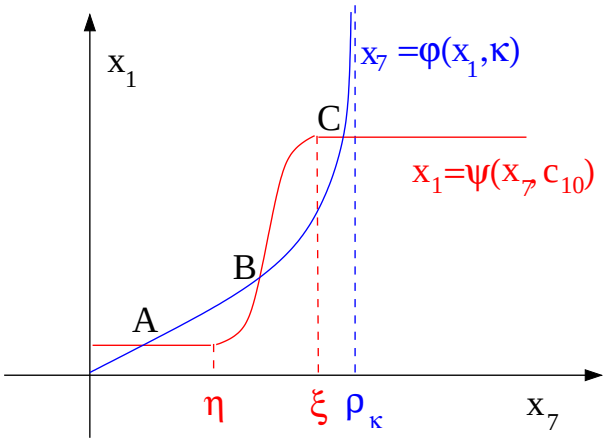

Fig. 6. The functions φ and ψ and their intersections

- For large values of κ, in particular for $\kappa \geq \xi$ two new equilibria may appear (points B and C in Figure 6). Such equilibria are more likely to appear when c_{10} is sufficiently large.

In the next subsection we will investigate the stability of the equilibria.

B. Bi-stability and hysteresis of the NGF-induced MAPK topology

We will analyze stability by assuming at most three equilibria, which we categorize as follows:

A-type: Equilibria achieved for $\bar{x}_7 < \eta$ (point A in Figure 6).
C-type: Equilibria achieved for $\bar{x}_7 > \xi$ (point C in Figure 6).
B-type: Equilibria appearing for $\eta < \bar{x}_7 < \xi$, between A-type and C-type steady states (point B in Figure 6).

Remark 3: It should be pointed out that, in principle, multiple equilibria in the range $\eta \leq \bar{x}_7 \leq \xi$ are possible. This case would be difficult to deal with without considering specific functions and values. However, we can conclude that this would be a "fragile" situation anyway. Indeed ψ has a "high slope" in the interval $[\eta, \xi]$. Thus multiple equilibria in $[\eta, \xi]$ means that the two curves have about the same slope, which implies fragility in the sense that these equilibria might disappear for small input variations.

The first result concerns the stability of points A and C.

Proposition 4: Equilibria occurring for $\bar{x}_7 < \eta$ (A-type) and $\bar{x}_7 > \xi$ (C-type) are locally stable.

Proof The proof is an extension to of the case reported in [12] Proposition 6..

If $\bar{x}_7 < \eta$, then $c_{17}(\bar{x}_7) = 0$ and the variable x_1 is not affected by x_7, i.e. the feedback is not active. Therefore, the system is a cascade of the x_1, the x_2–x_4 and the x_5–x_6–x_7.

It is immediate that x_1 stably converge to its equilibrium $\bar{x}_1$. The stability of subsystem x_2–x_4 can be immediately seen by considering the Jacobian, written in the appendix (eq. (49)) (see [12] for details). Then also x_2–x_4 converge to their steady–state values.

We need to show the stability of the x_5–x_6–x_7 subsystem for fixed x_1 and x_4. Consider expressions (30), (32) and (38), and recall that $\zeta = x_5 + x_6 + x_7$:

$$\begin{aligned} \dot{x}_5 &= c_{56}(\zeta - x_5 - x_7) - b_{54}(x_5)x_4 + c_{51}(x_1) - b_{55}(x_5)x_5 \\ \dot{\zeta} &= c_{51}(x_1) - b_{55}(x_5)x_5 \\ \dot{x}_7 &= a_{74}(\zeta - x_5 - x_7)x_4 - b_{77}(x_7)x_7 \end{aligned}$$

The Jacobian turns out to be

$$J = \begin{bmatrix} -[(b_{55}(x_5)x_5)' + b'_{54}\bar{x}_4 + c'_{56}] & c'_{56} & -c'_{56} \\ -(b_{55}(x_5)x_5)' & 0 & 0 \\ -a'_{74} & a'_{74} & -[a'_{74}\bar{x}_4 + (b_{77}(x_7)x_7)'] \end{bmatrix}$$

Apply the following similarity transformations: T_1) add column 1 to column 2 and subtract row 2 from row 1; T_2) change sign to the first row and column. We achieve the similar matrix

$$J = \begin{bmatrix} -[b'_{54}\bar{x}_4 + c'_{56}] & +b'_{54}\bar{x}_4 & +c'_{56} \\ +(b_{55}(x_5)x_5)' & -(b_{55}(x_5)x_5)' & 0 \\ +a'_{74} & 0 & -[a'_{74} + (b_{77}(x_7)x_7)'] \end{bmatrix}$$

Stability of this matrix can be proven in several ways. First, the matrix is weakly diagonally dominant with negative diagonal elements and with the third row strictly dominant. Otherwise one can see that the matrix is Metzler (it has nonnegative non–diagonal entries) and so it is stable if and only if the characteristic polynomial has positive coefficients. This condition is indeed fulfilled by our system. □

The previous result is not surprising, since it is known that the MAPK is open–loop stable and monotone. Several results along this line have been derived based on graph–theoretic considerations and Hill–type models [9], [21]. Similarly one could prove that points of B-type, for $\eta < \bar{x}_7 < \xi$, are necessarily unstable. We do not provide here a formal proof, which would be along the lines of the results in [9]).

The result we prove in the next paragraphs is instead of a different nature, since we are able to prove global stability of the system adopting a Lyapunov function for the x_5–x_6–x_7 subsystem. This result is quite useful to prove the possibility of hysteresis.

Theorem 2: For fixed values of $\bar{x}_1$ and $\bar{x}_4$, the equilibrium point $\bar{x}_5$–$\bar{x}_6$–$\bar{x}_7$ of the subsystem governed by (30) (31) and (32) is globally stable and, denoting by $z_5 = x_5 - \bar{x}_5$, $z_6 = x_6 - \bar{x}_6$, $z_7 = x_7 - \bar{x}_7$, it admits the polyhedral (see [22], [23]) Lyapunov function

$$V(z_5, z_6-, z_7) = \max\{|z_5 + z_6 + z_7|, |z_6 + z_7|, |z_7|\}$$

The proof is reported in the Appendix.

We can also prove the following corollary:

Corollary 1: The sets

$$\mathcal{Z}^+ = \{z_5, z_6, z_7 : \quad z_5 + z_6 + z_7 \geq 0,\ z_6 + z_7 \geq 0,\ z_7 \geq 0\}$$

and

$$\mathcal{Z}^- = \{z_5, z_6, z_7 : \quad z_5 + z_6 + z_7 \leq 0,\ z_6 + z_7 \leq 0,\ z_7 \leq 0\}$$

are positively invariant. Moreover, using the same notation introduced for Theorem 2, assume that x_1 and x_4 are perturbed to $x_1 > \bar{x}_1$ and $x_4 > \bar{x}_4$. Then $\mathcal{Z}^+$ remains positively invariant.

The proof is reported in the Appendix.

Theorem 2 and Corollary 1 have an important consequence. Assume that the input is low and that the system is at a relaxed, A-type, steady state for x_7. Assume also that, at the same time, $\bar{x}_7 > \xi$ is an admissible equilibrium. Then, if the input is increased enough to bring the state in the $\mathcal{Z}^+$ then the output will remain at the high level even after removal of the input stimulus. Loosely speaking, a temporary but sufficiently high injection of c_{10} will shift the stable equilibrium of x_7 to a high value, $x_7 > \xi$. To be more precise we formalize this concept in the following proposition.

Proposition 5: Let $\bar{c}_{10}$ an input value for which both a $\bar{x}_7 < \eta$ and $\bar{x}_7 > \xi$ equilibria are admissible (namely, κ is large enough to assure the existence of an equilibrium $\bar{x}_7 > \xi$). Let $\bar{x}_1$ and $\bar{x}_4$ the corresponding steady state-levels of x_1 and x_4 and let $\mathcal{Z}^+$ be the corresponding invariant set, as defined in Corollary 1. If the input

c_{10} is large enough to bring the state in $\mathcal{Z}^+$, x_4 above $\bar{x}_4$ and x_1 above $\bar{x}_1$, then the system will converge to $\bar{x}_7 > \xi$, even after removal of the input c_{10}.

Proof It is a simple matter of noticing that $\mathcal{Z}^+$ is invariant and in such region, $c_{17}(x_7)$ is constant. Then both x_1 and x_4 converge to their steady state from above. Convergence is assured by Theorem 2. □

Remark 4: The equilibrium $\bar{x}_7 > \xi$ is maintained even after the input is removed, under the assumption $x_2 + x_3 + x_4 = \kappa$, where κ is constant. The latter is a reasonable assumption in the short term, since we hypothesize mass conservation for the $MAP2K$ protein, or slowly varying total $MAP2K$ concentration. Our model predicts that if degradation is taken into account and in the long run $\dot{\kappa} < 0$, then this could lead to the situation in which the high x_7 equilibrium cannot be sustained and the system is reset to a low x_7 amount. The overall situation is depicted in Figure 7. If the system is in a low stable concentration of x_7, (left–top), a step in the input can shift the equilibrium to a high value (right–top). After restoring the input to zero (left–bottom), the system will remain in a high x_7 equilibrium. If there is a decrease of the total available amount of $MAP2K = x_2 + x_3 + x_4$, then the x_7 output is driven back to a low value (right–bottom).

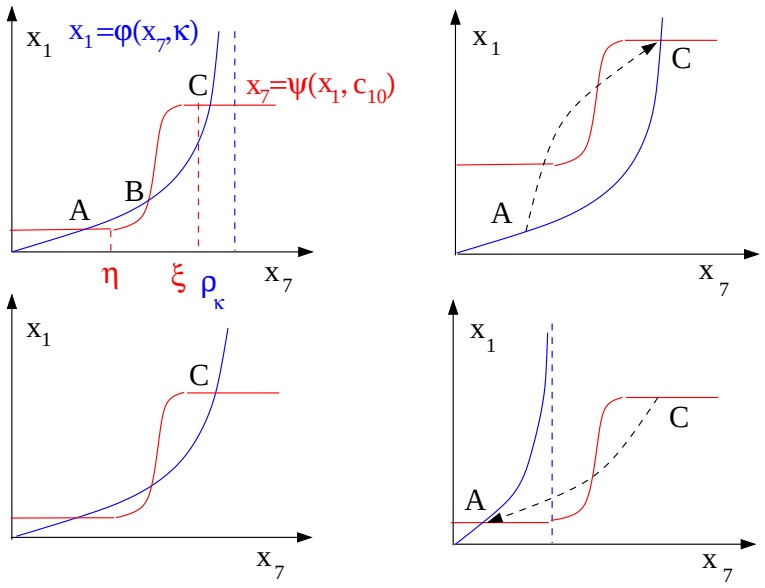

Fig. 7. Possible equilibria configurations for the NGF-induced topology. Left–top: uninduced system, low x_7 concentration; Right–top: sustained double phosphorylation for the MAP1K output; Left–bottom: hysteresis, the equilibrium of x_7 concentration remains high after removal of the input; Right–bottom: relaxation of the equilibrium of x_7 to low concentrations.

V. Conclusions

By means of the framework suggested in [12], we have examined two input-dependent topologies of the MAPK pathway, arising in PC12 neural cells [11]. Such topologies correspond to different dynamic behaviors of the MAPK pathway output and correspond to different cell fate decisions. We have proposed qualitative models that capture the essential feature of these systems, while neglecting specific parameter values for the chemical interactions within the network species. These models allowed us to demonstrate that the two topologies robustly exhibit the experimentally verified behaviors induced in the network by EGF and NGF inputs. To prove our results, we relied on classical control theoretic analysis, based on invariant set theory and Lyapunov functions, without the need for numerical simulations.

References

[1] Kitano, H., Systems biology: A brief overview. *Science* **295**, 1662–1664 (2002).

[2] Barkai, N. & Leibler, S., Robustness in simple biochemical networks. *Nature* **387**, 913–917 (1997).
[3] Alon, U., Surette, M. G., Barkai, N., & Leibler, S., Robustness in bacterial chemotaxis. *Nature* **397**, 168–171 (1999).
[4] Yi, T. M., Huang, Y., Simon, M. I., & Doyle, J., Robust perfect adaptation in bacterial chemotaxis through integral feedback control. *Proceedings Of The National Academy Of Sciences Of The United States Of America* **97**, 4649–4653 (2000).
[5] El-Samad, H. J. C. M., H—Kurata, Surviving heat shock: Control strategies for robustness and performance. *Proceedings of the National Academy of Sciences of the United States of America* **102**, 2736–2741 (2005).
[6] Shinar, G., Milo, R., Rodrìguez Martìnez, M., & Alon, U., Input-output robustness in simple bacterial signaling systems. *Proceedings of the National Academy of Sciences* **104**, 19931–199935 (2007).
[7] Shinar, G. & Feinberg, M., Structural sources of robustness in biochemical reaction networks. *Science* **327**, 1389–1391 (2010).
[8] Ferrell, J., James E. & Machleder, E. M., The Biochemical Basis of an All-or-None Cell Fate Switch in Xenopus Oocytes. *Science* **280**, 895–898 (1998).
[9] Angeli, D., Ferrell, J. E., & Sontag, E. D., Detection of multistability, bifurcations, and hysteresis in a large class of biological positive-feedback systems. *Proceedings of the National Academy of Sciences of the United States of America* **101**, 1822–1827 (2004).
[10] Angeli, D. & Sontag, E., Monotone control systems. *IEEE Trans. Automat. Control* **48**, 1684–1698 (2003), errata are here: http://www.math.rutgers.edu/(tilde)sontag/FTPDIR/angeli-sontag-monotone-TAC03-typos.txt.
[11] Santos, S. D. M., Verveer, P. J., & Bastiaens, P. I. H., Growth factor-induced mapk network topology shapes erk response determining pc-12 cell fate. *Nat Cell Biol* **9**, 324–330 (2007).
[12] Blanchini, F. & Franco, E., Structurally robust biological networks. *Submitted (available for download at www.cds.caltech.edu/∼elisa/BlaFra2010.html)* (2010).
[13] Sontag, E., Monotone and near-monotone biochemical networks. *Systems and Synthetic Biology* **1**, 59–87 (2007).
[14] Chesi, G. & Hung, Y., Stability analysis of uncertain genetic sum regulatory networks. *Automatica* **44**, 2298–2305 (2008).
[15] Radde, N., Bar, N., & Banaji, M., Graphical methods for analysing feedback in biological networks - a survey. *Int. J. Syst. Sci.* **41**, 35–46 (2010).
[16] El-Samad, H., Prajna, S., Papachristodoulou, A., Doyle, J., & Khammash, M., Advanced methods and algorithms for biological networks analysis. *Proceedings of the IEEE* **94**, 832–853 (2006).
[17] Feinberg, M., Chemical reaction network structure and the stability of complex isothermal reactors I. the deficiency zero and deficiency one theorems. *Chemical Engineering Science* **42**, 2229–2268 (1987).
[18] Prill, R. J., Iglesias, P. A., & Levchenko, A., Dynamic properties of network motifs contribute to biological network organization. *PLoS Biology* **3**, e343 (2005).
[19] Ma, W., Trusina, A., El-Samad, H., Lim, W. A., & Tang, C., Defining network topologies that can achieve biochemical adaptation. *Cell* **138**, 760–773 (2009).
[20] Kholodenko, B. N., Kiyatkin, A., Bruggeman, F. J., Sontag, E., Westerhoff, H. V., & Hoek, J. B., Untangling the wires: A strategy to trace functional interactions in signaling and gene networks. *Proceedings of the National Academy of Sciences* **99**, 12841–12846 (2002).
[21] Wang, L. & Sontag, E., Singularly perturbed monotone systems and an application to double phosphorylation cycles. *J. Nonlinear Sciences* (2008).
[22] Blanchini, F., Set invariance in control – a survey. *Automatica* **35**, 1747–1767 (1999).
[23] Blanchini, F. & Miani, S., *Set-theoretic methods in control*, volume 22 (Boston: Birkhäuser, 2008), Systems & Control: Foundations & Applications.

APPENDIX

A. Proof of Lemma 1

Consider the equations (3)–(6) that implicitly define x_i, $i = 1, ..., 4$, as functions of x_7 and c_{10}. We can replace the equation (5) by (7) (namely $\dot{\kappa} = 0$). Also, in view of (7), (4) can be rewritten as (46) below.

$$+ c_{10} - b_{11}(x_1)x_1 = -d_{17}(x_7) \quad (45)$$
$$-b_{21}(x_2)x_1 + c_{23}(x_3) = 0 \quad (46)$$
$$-b_{22}(x_2)x_2 = -d_{27}(x_7) \quad (47)$$
$$a_{41}(x_3)x_1 - b_{44}(x_4)x_4 = 0 \quad (48)$$

The Jacobian J of the transformation is

$$J = \begin{bmatrix} -(b11(x_1)x_1)' & 0 & 0 & 0 \\ -b_{21}(x_2) & -b'_{21}(x_2)x_1 & c'_{23}(x_3) & 0 \\ 0 & -(b22(x_2)x_2)' & 0 & 0 \\ a_{41}(x_3) & 0 & a'_{41}(x_3)x_1 & -(b_{44}(x_4)x_4)' \end{bmatrix}$$

The sign matrix is

$$sign(J) = \begin{bmatrix} - & 0 & 0 & 0 \\ - & - & + & 0 \\ 0 & - & 0 & 0 \\ + & 0 & + & - \end{bmatrix}$$

The determinant of such a Jacobian is positive and thus the function φ is well defined.

The proof could proceed with tedious derivative computation. We give here a simple qualitative reasoning.

Assume that x_7 increases for constant c_{10}. Then $-d_{17}(x_7)$ increases. From (47) we have that x_2 does not increase. Since $c_{10} = const$ and $-d_{17}(x_7)$ increases, from (45), we have that x_1 must decrease. If x_1 decreases, from (46) x_3 must also decrease. From (48), a decrease of x_3 and x_1 causes a decrease of x_4.

Assume that c_{10} increases with constant x_7. Then x_2 is constant by (47). From (45), x_1 must increase. If x_1 increases x_3 increases by (46) and, finally, x_4 increases by (48).

B. Proof of Lemma 4

The Jacobian of the transformation with respect to x_2 and x_4 is

$$J = \begin{bmatrix} -(b'_{21}(x_2)x_1 + c'_{23}) & c'_{23} \\ -a'_{41}x_1 & -(a'_{41}x_1 + (b_{44}(x_4)x_4)') \end{bmatrix} \tag{49}$$

and is invertible. Thus x_2 and x_4 are well defined functions.

To prove that φ is increasing, note that since

$$b_{21}(x_2)x_1 = c_{23}(k - x_2 - x_4)$$

x_1 increasing implies either x_4 increasing or x_2 decreasing. In the first case, we are done, otherwise, we note that from

$$a_{41}(k - x_2 - x_4)x_1 = b_{44}(x_4)x_4$$

x_2 decreasing implies x_4 increasing.

Similarly, since the argument $k - x_2 - x_4$ appears in bot equations, for x_1 constant, we have that x_2 or x_4 or both decrease or both increase. The first equation imposes that if κ increases, then either x_2 or x_4 must increase. □

C. Proof of Theorem 2 and Corollary 2

Let $\bar{x}_1$ and $\bar{x}_4$ and $\bar{c}_{51} = c_{51}(\bar{x}_1)$ be fixed. Consider the variables $\zeta = x_5 + x_6 + x_7$, $\omega = x_7$ and

$$\sigma = x_6 + x_7 = \zeta - x_5$$

so that $x_5 = \zeta - \sigma$, $x_6 = \sigma - \omega$. From (30)–(32) we have

$$\dot{\zeta} = -b_{55}(\zeta - \sigma)(\zeta - \sigma) + \bar{c}_{51} \tag{50}$$
$$\dot{\sigma} = a_{64}(\zeta - \sigma)\bar{x}_4 - b_{66}(\sigma - \omega)(\sigma - \omega) \tag{51}$$
$$\dot{\omega} = a_{74}(\zeta - \omega) - b_{77}(\omega)\omega \tag{52}$$

The steady state conditions are

$$0 = -b_{55}(\bar{\zeta} - \bar{\sigma})(\bar{\zeta} - \bar{\sigma}) + \bar{c}_{51} \tag{53}$$
$$0 = a_{64}(\bar{\zeta} - \bar{\sigma})\bar{x}_4 - b_{66}(\bar{\sigma} - \bar{\omega})(\bar{\sigma} - \bar{\omega}) \tag{54}$$
$$0 = a_{74}(\bar{\zeta} - \bar{\omega}) - b_{77}(\bar{\omega})\bar{\omega} \tag{55}$$

The candidate Lyapunov function in the new variables is

$$V = \max\{|z_5 + z_6 + z_7|, |z_6 + z_7|, |z_7|\} = \max\{\pm(\zeta - \bar{\zeta}), \pm(\sigma - \bar{\sigma}), \pm(\omega - \bar{\omega})\}$$

To prove both Theorem and Corollary we split V in two components as $V = \max\{V_-, V_+\}$. Let

$$V_- = \max\{-(\zeta - \bar{\zeta}), -(\sigma - \bar{\sigma}), -(\omega - \bar{\omega}), 0\}$$

then we show that V_- decreases until the set in which it is 0, namely $\zeta \geq \bar{\zeta}$, $\sigma \geq \bar{\sigma}$ and $\omega \geq \bar{\omega}$ is reached.

Outside this set we distinguish three regions in each of which V_- is equal to one of its affine components.

ζ–region: $V_- = -(\zeta - \bar{\zeta})$. Here we necessarily have $-(\zeta - \bar{\zeta}) \geq -(\sigma - \bar{\sigma})$ then

$$\zeta - \sigma \leq \bar{\zeta} - \bar{\sigma}$$

The derivative is (note that $\bar{c}_{51} - c_{51}(\bar{x}_1) = 0$):

$$\frac{d}{dt}(\bar{\zeta} - \zeta) = -\dot{\zeta} = +[b_{55}(\zeta - \sigma)(\zeta - \sigma) - b_{55}(\bar{\zeta} - \bar{\sigma})(\bar{\zeta} - \bar{\sigma})] + \bar{c}_{51} - c_{51}(\bar{x}_1) < 0 \tag{56}$$

unless $\zeta - \sigma = \bar{\zeta} - \bar{\sigma}$ for which the equality holds $\dot{\zeta} = 0$.

σ–region: $V_- = \bar{\sigma} - \sigma$. As above here we have $-(\sigma - \bar{\sigma}) \geq -(\zeta - \bar{\zeta})$ and $-(\sigma - \bar{\sigma}) \geq -(\omega - \bar{\omega})$:

$$\sigma - \zeta \leq \bar{\sigma} - \bar{\zeta}, \quad \sigma - \omega \leq \bar{\sigma} - \bar{\omega},$$

then (we assume $x_4 = \bar{x}_4$)

$$\frac{d}{dt}(\bar{\sigma} - \sigma) = -\dot{\sigma} = -[a_{64}(\zeta - \sigma)x_4 - a_{64}(\bar{\zeta} - \bar{\sigma})\bar{x}_4] + [b_{66}(\sigma - \omega)(\sigma - \omega) - b_{66}(\bar{\sigma} - \bar{\omega})(\bar{\sigma} - \bar{\omega})] < 0 \tag{57}$$

unless $\sigma - \bar{\sigma} = \zeta - \bar{\zeta} = \omega - \bar{\omega}$, for which case $\sigma = 0$.

ω–region: $V = -(\omega - \bar{\omega})$. Here we have $-(\omega - \bar{\omega}) \geq -(\zeta - \bar{\zeta})$ and $-(\omega - \bar{\omega}) > 0$:

$$\omega - \zeta \leq \bar{\omega} - \bar{\zeta}, \quad \omega < \bar{\omega},$$

then (again we assume $x_4 = \bar{x}_4$)

$$\frac{d}{dt}(\bar{\omega} - \omega) = -\dot{\omega} = -[a_{74}(\zeta - \omega)x_4 - a_{74}(\bar{\zeta} - \bar{\omega})\bar{x}_4] + [b_{77}(\omega)\omega - b_{77}(\bar{\omega})\bar{\omega}] < 0 \tag{58}$$

unless $\omega - \bar{\omega} = \zeta - \bar{\zeta}$ and $\omega = \bar{\omega}$, for which case $\dot{\omega} = 0$.

Since its derivative is non–positive, V_- is never increasing. To show that it is decreasing, unless for $V_- = 0$, we consider the fact that its derivative is negative, unless the evidenced special conditions, in which the derivative is zero, occur. We need then to use Krasowskii arguments to show that these conditions do not persist for $V_- > 0$, precisely, it they happen at $\bar{t}$, they will not be true in a right neighborhood $\bar{t} < t \leq \bar{t} + \epsilon$.

The critical condition $\dot{\zeta} = 0$ in the ζ–region, namely $\zeta - \bar{\zeta} = \sigma - \bar{\sigma}$, is only possible at the boundary with the σ–region. Permanence of the situation, would imply that also $\dot{\sigma} = 0$, which is possible only at the intersection of the previous regions with the ω–region, namely $\zeta - \bar{\zeta} = \sigma - \bar{\sigma} = \omega - \bar{\omega}$. Again this condition can endure only if also $\dot{\omega} = 0$. Then the critical condition is persistent only if $\dot{\zeta} = \dot{\sigma} = \dot{\omega} = 0$, hence $V_- = 0$.

Similar considerations show that also the critical situations evidenced for the σ–region and for the ω–region cannot endure.

The fact that V_- is decreasing, implies that $\zeta(t), \sigma(t), \omega(t)$, converge to the region $\zeta \geq \bar{\zeta}$, $\sigma \geq \bar{\sigma}$ and $\omega \geq \bar{\omega}$.

Exactly in the same way we can prove that

$$V_+ = \max\{+(\zeta - \bar{\zeta}), +(\sigma - \bar{\sigma}), +(\omega - \bar{\omega}), 0\}$$

is decreasing, hence that the original $V = \max\{V_+, V_-\}$ is decreasing.

The first part of of Corollary 1 is proven, because we have seen that V_- (V_+) is non–increasing, thus set $\mathcal{Z}^-$ ($\mathcal{Z}^+$) cannot be escaped.

We have just to prove that $\mathcal{Z}^+$ remains invariant also if we increase x_1 and x_4. This is quite easy, since if we take $x_1 > \bar{x}_1$ and $x_4 > \bar{x}_4$ the inequalities (56), (58) and (57) still hold. □